Electronic Supporting Information

Spin-orbit coupling is the key to unraveling intriguing features of halogen bond with astatine

Elisa Rossi,[a] Matteo De Santis,[a] Diego Sorbelli,[a] Loriano Storchi[bc], Leonardo Belpassi[bd], Paola Belanzoni[abd]**

[a] *Department of Chemistry, Biology and Biotechnology, University of Perugia, via Elce di Sotto 8, 06123 Perugia, Italy E-mail: paola.belanzoni@unipg.it*

[b] *CNR Institute of Chemical Science and Technologies "Giulio Natta" (CNR-SCITEC), via Elce di Sotto 8, 06123 Perugia, Italy*

[c] *Dipartimento di Farmacia , Università G. D'Annunzio, via dei Vestini 31, 66100 Chieti, Italy*

[d] *Consortium for Computational Molecular and Materials Sciences (CMS)2, via Elce di Sotto 8, 06123 Perugia, Italy*

Benchmark study

To set up the most accurate and efficient computational protocol for the systematic study on the Cl—X ⋯ NH_3 (X = Cl, Br, I and At) adducts, preliminary benchmark calculations have been performed. The frozen core approximation, basis set size, integration accuracy and functional type parameters have been tested for assessing the accuracy of bonding energies, equilibrium geometries and CT values in the CD analysis, at both ZORA scalar and ZORA SOC level of theory. The Cl—At ⋯ NH_3 adduct has been chosen as test case, whereas the whole adduct series has been considered for the exchange-correlation functional validation study. Since experimental data are not available, results are compared with bonding energies and geometrical parameters reported in the literature, calculated with the scalar relativistic explicitly correlated counterpoise corrected CCSD(T)-F12b/VTZ-F12 method[1] the scalar (sr-) and spin-orbit including (2c-) relativistic PW6B95/AVTZ DFT methods[2], also exploring 36 different DFT functionals.

1 The frozen core approximation

The basis set functions used in the ADF program[3] are Slater Type Orbitals (STOs). A basis set can roughly be characterized by the level of frozen core approximation and by its size (single-, double-, triple-zeta; with or without polarization). The frozen core approximation allows for explicitly including only valence electrons in the calculations. Different levels of frozen core approximations can be used in ADF: none, corresponding to all electron calculations, small and large.

1.1 Bonding energies

In Table S1 the bonding energies between Cl—At and NH_3 in the Cl—At ⋯ NH_3 adduct calculated at both ZORA scalar and ZORA SOC level with all electrons (core none), small frozen core (core small, Cl: 1s-2p; N: 1s; At: 1s-4d) and large frozen core (core large, Cl: 1s-2p; N: 1s; At: 1s-5d) approximation are reported. Values taken from references 1 and 2 are also shown for comparison.

	Core none	Core small	Core large	Literature values
Scalar	**-16.62**	**-16.50**	**-15.83**	**-15.36** [1]
SOC	**(-13.97)**	**(-14.86)**	**(-14.03)**	**(-13.30)** [2]
ΔSO	**2.65**	**1.64**	**1.80**	**2.37** [2]

Table S1: Bonding energies (scalar ZORA and ZORA SOC) (kcal/mol) between Cl—At and NH_3 in Cl—At $\cdots NH_3$. All calculations have been done with the GGA BP86 functional and the ZORA/TZ2P basis set. Literature values are: counterpoise corrected CCSD(T)-F12b/VTZ-F12 stabilization energy[1] and sr-PW6B95/AVTZ stabilization energy[2].

It can be observed that the change in the values, due to the different frozen core approximation used, is within the same order of magnitude as the SOC effects (ΔSO). Neither convergence with the different frozen core approximations or a clear trend in the bonding energies can be found.

On the basis of these findings it is clear that the bonding energy largely depends on the frozen core approximation. In addition, the calculated trend of the scalar values (i.e. values decreasing on increasing the core size) is not reproduced for the SOC ones. The reason for that can be found in the fact that in the ZORA SOC calculations the ADF program uses a scalar type core. All the calculations performed by employing a frozen core approximation different from core none, at the SOC level, are therefore "hybrid" calculations, where the core electrons are treated at the scalar ZORA level and the valence electrons are treated at the ZORA SOC one. This result is noteworthy because it would highlight a strong SOC coupling effect on the core description of astatine, suggesting that in this case the polarization of the core electrons cannot be neglected by using a "scalar" core.

To confirm this assumption the bonding energy between Cl—Br and NH_3 in the Cl—Br $\cdots NH_3$ adduct has been calculated with the same computational set-up and results are shown in Table S2.

	Core none	**Core small**	**Core large**	**Literature values**
Scalar	**-12.87**	**-12.67**	**-12.19**	**-9.06** [1]
SOC	**(-12.83)**	**(-12.63)**	**(-12.15)**	**/**
ΔSO	**0.04**	**0.04**	**0.04**	**/**

Table S2: Bonding energies (scalar ZORA and ZORA SOC) (kcal/mol) between Cl-Br and NH_3 in Cl—Br $\cdots NH_3$. All calculations have been done with the GGA BP86 functional and the ZORA/TZ2P basis set. Literature values are: counterpoise corrected CCSD(T)-F12b/VTZ-F12 stabilization energy[1]. The SOC value of the stabilization energy is not available in the literature.

These values clearly support the result that the SOC largely affects the core description of astatine. Indeed, as shown in Table S2, bromine core is not affected by spin-orbit coupling and the values trend found at the scalar ZORA level is also reproduced at the ZORA SOC one.

A comparison of the calculated Cl—At$\cdots NH_3$ and Cl—Br $\cdots NH_3$ bonding energies with those reported in the literature shows that the scalar ZORA values are sizably larger, particularly for Cl—Br $\cdots NH_3$, than those calculated at the counterpoise corrected CCSD(T)-F12b/VTZ-F12 level[1], whereas the SOC value for Cl—At $\cdots NH_3$ is only slightly larger than that calculated at the DFT sr-PW6B95/AVTZ level.

In conclusion, the frozen core approximation can be tested only at the scalar ZORA level. The bonding energy values heavily depend on the core, showing an increase with decreasing core size, with the largest value obtained in the all electron calculation.

1.2 Geometry

The frozen core approximation effect on the equilibrium geometry has been studied in the Cl—At ···NH_3 and Cl—Br ···NH_3 adducts. In Table S3 the optimized bond distances calculated at the scalar ZORA level with the different frozen core approximations (core none, core small and core large) are reported.

	Core None		**Core Small**		**Core Large**		**Literature values**	
Cl—At ···NH_3	**Cl—At**	**At···N**	**Cl—At**	**At···N**	**Cl—At**	**At···N**	**Cl—At**	**At···N**
	2.522	**2.627**	**2.526**	**2.632**	**2.558**	**2.660**	**2.479** [1]	**2.630** [1]
Cl—Br ···NH_3	**Cl—Br**	**Br···N**	**Cl—Br**	**Br···N**	**Cl—Br**	**Br···N**	**Cl—Br**	**Br···N**
	2.268	**2.426**	**2.271**	**2.431**	**2.290**	**2.465**	**2.194** [1]	**2.529** [1]

Table S3: Distances (Å) in the Cl—At···NH_3 and Cl—Br ··· NH_3 adducts. All the calculations have been done at the ZORA scalar level with the GGA BP86 functional and the ZORA/TZ2P basis set. Literature values are: counterpoise corrected CCSD(T)-F12b /VTZ-F12 optimized intermolecular and intrahalogen bond lengths (Å)[1].

The optimized bond distances show only a small dependence on the core size, slightly decreasing with decreasing the core size. Convergence with the different frozen core approximations can be found, since corresponding core small and core none bond distance values are very close. Compared to the literature values, a good agreement can be observed for the At···N distance, whereas the Cl—At and Cl—Br bond lengths are slightly longer and the Br···N distance is slightly shorter.

1.3 Charge Displacement analysis

To study the frozen core approximation effect on the CD analysis, the CD curves have been calculated using core none, core small and core large at scalar ZORA level for the Cl—At···NH_3 adduct and they are compared in Figure S1.

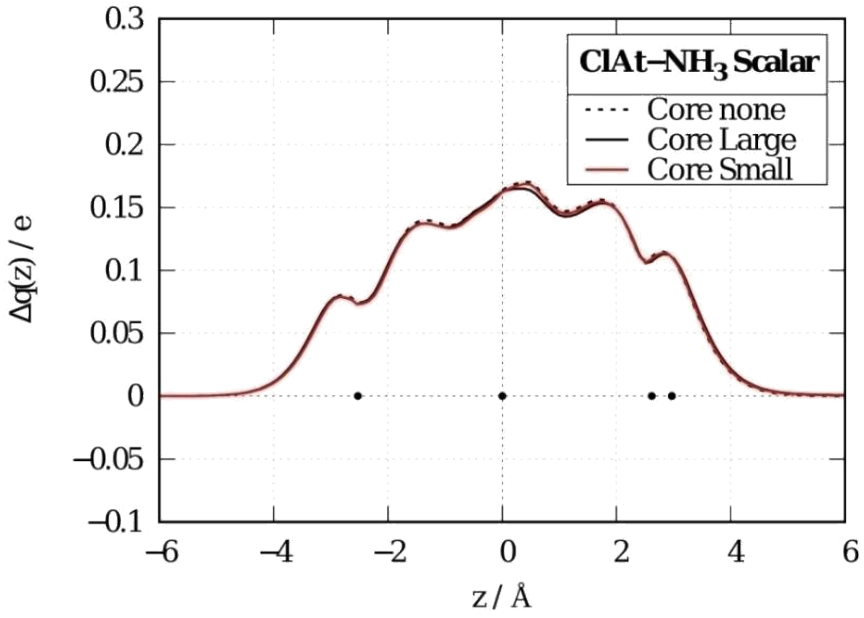

Figure S1: Charge displacement curves for Cl—At ···NH_3 at scalar ZORA level. All the calculations have been done with the GGA BP86 functional and the ZORA/TZ2P basis set. Black points represent, from the left to the right, the positions of the Cl, At, N and H atoms, respectively, at the core none geometry.

The three CD curves overlap in Figure S1 indicates that the frozen core approximation does not affect the CD analysis. The positive sign of the curves shows an electron charge flow from NH_3 to At in the Cl—At fragment. The corresponding Charge Transfer CT values calculated at the isodensity boundary are reported in Table S4 and they are also very close.

	Core none CT(e)	Core small CT(e)	Core large CT(e)
Scalar	**0.151**	**0.149**	**0.147**

Table S4: Charge transfer values (CT) (electrons) obtained from the CD analysis at scalar ZORA level for the Cl—At ···NH_3 adduct. All the calculations have been done with the GGA BP86 functional and the ZORA/TZ2P basis set.

CD curves calculated at scalar ZORA and ZORA SOC level for the Cl—At ···NH_3 adduct using core none are compared in Figure S2. We recall here that only core none, namely all electron calculation, can be employed for including SOC effects, due to the poor description of astatine core electrons by scalar type cores. It is evident that inclusion of SOC sizably affects the CD curve.

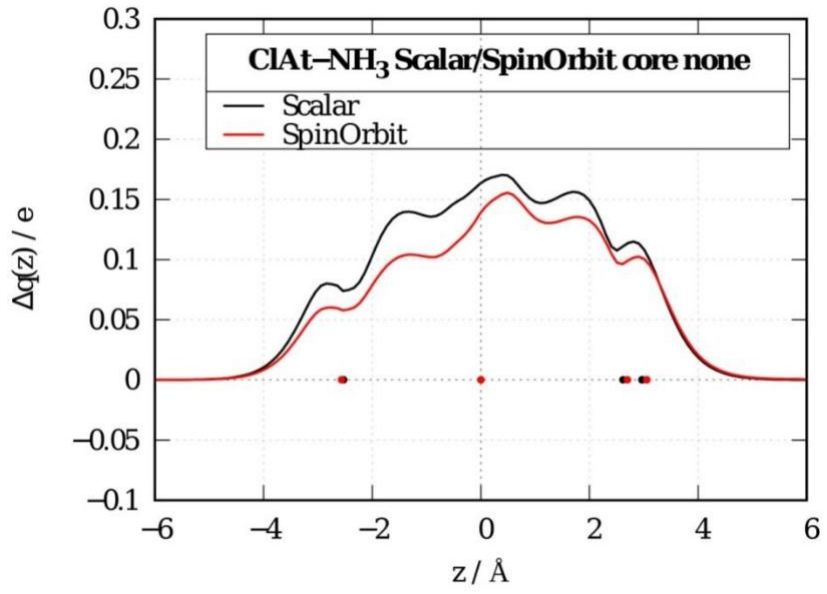

Figure S2: Charge displacement curves for Cl—At ···NH_3 at scalar ZORA and ZORA

SOC level using core none. All the calculations have been done with the GGA BP86 functional and the ZORA/TZ2P basis set. Black/red points represent, from the left to the right, the positions of the Cl, At, N and H atoms at the core none scalar geometry and SOC geometry, respectively.

On the basis of all these results, showing sizable SOC effects on the core description of astatine, we chose to perform all electron calculations (core none) in our systematic study.

2 The basis set effect

Basis sets typically come in hierarchies of increasing size, giving a controlled way to obtain more accurate results, however at a higher computational cost. ZORA relativistic calculations have special basis set requirements, especially in the core region. ZORA basis sets with frozen core should be used exclusively in relativistic calculations with the ZORA approach, while all electron ZORA basis sets can be used for both relativistic and non-relativistic calculations. Usually the ZORA basis sets contain much steeper basis and fit functions to accurately describe the core region. The ZORA/TZ2P basis set is made by a core double zeta, a valence triple zeta, and two extra polarization functions. The ZORA/TZ2P basis set files are available in ADF for all the elements.

The ZORA/QZ4P basis set can be described as core triple zeta, valence quadruple zeta, with four sets of polarization functions. ZORA/QZ4P is a large basis set that, for example, is made by 21 functions for the hydrogen atom, compared to 11 functions constituting the ZORA/TZ2P basis set for the hydrogen. The effect of the basis set size will be studied only at all electron level, with calculations based on the core none. The reason for this choice is that for the ZORA/QZ4P basis sets only all electron basis sets are available**.**

2.1 Bonding energies

The bonding energies between Cl—At and NH_3 in the Cl—At···NH_3 adduct calculated

at both ZORA scalar and ZORA SOC level with all electrons (core none) ZORA/TZ2P and ZORA/QZ4P basis sets are reported in Table S5. Values taken from references 1 and 2 are also shown for comparison.

	TZ2P	**QZ4P**	**Literature values**
	BE (kcal/mol)	**BE (kcal/mol)**	
Scalar	**-16.62**	**-16.95**	**-15.36** [1]
SOC	**(-13.97)**	**(-13.96)**	**(-13.30)** [2]
ΔSO	**2.65**	**2.99**	**2.37** [2]

Table S5: Bonding energies (scalar ZORA and ZORA SOC) (kcal/mol) between Cl—At and NH_3 in the Cl—At $\cdots NH_3$ adduct. Calculations have been done with the GGA BP86 functional and the all electron ZORA/TZ2P and ZORA/QZ4P basis sets. Literature values are: counterpoise corrected CCSD(T)-F12b/VTZ-F12 stabilization energy[1] and sr-PW6B95/AVTZ stabilization energy[2].

From Table S5 it is clear that convergence with the different basis set sizes cannot be found. In particular, the difference between scalar ZORA and ZORA SOC values (ΔSO) increases on increasing the basis set size (see ZORA/QZ4P results).

These findings suggest that further analysis could be needed by testing the integration quality to understand if the variability of the bonding energies could be related to that. The results of the test on the numerical quality will be presented in the next section.

2.2 Geometry

The basis set size effect on the equilibrium geometry has been studied in the Cl—At···NH_3 adduct. Table S6 summarizes the optimized bond distances calculated at both the scalar ZORA and ZORA SOC level using the TZ2P and QZ4P basis sets.

	TZ2P		**QZ4P**		**Literature**	**Values**
	Cl-At	**At···N**	**Cl-At**	**At···N**	**Cl—At**	**At···N**
Scalar	**2.522**	**2.627**	**2.524**	**2.615**	**2.479** [1]	**2.630** [1]
SOC	**(2.564)**	**(2.700)**	**(2.571)**	**(2.689)**	**(2.536)** [2]	**(2.693)** [2]
ΔSO	**0.042**	**0.073**	**0.047**	**0.074**	**0.045** [2]	**0.078** [2]

Table S6: Distances (Å) in the Cl—At···NH_3 adduct. All the calculations have been done with the GGA BP86 functional and core none. Literature values are: counterpoise corrected CCSD(T)-F12b /VTZ-F12 optimized intermolecular and intrahalogen bond lengths (Å) [1] .

We can see that the basis set size effect on the geometry is not so large as on the bonding energy. From the tabulated values it also emerges that on increasing the basis set size larger spin-orbit coupling effects are found. As a general trend, all the distances get slightly longer by using the larger ZORA/QZ4P basis set.

2.3 Charge Displacement analysis

The basis set size effect on the CD analysis is illustrated in Figures S3 and S4. The CD curves have been calculated using ZORA/TZ2P and ZORA/QZ4P basis sets with core none at scalar ZORA level (Figure S3) and ZORA SOC (Figure S4) for the Cl—At ⋯NH_3 adduct.

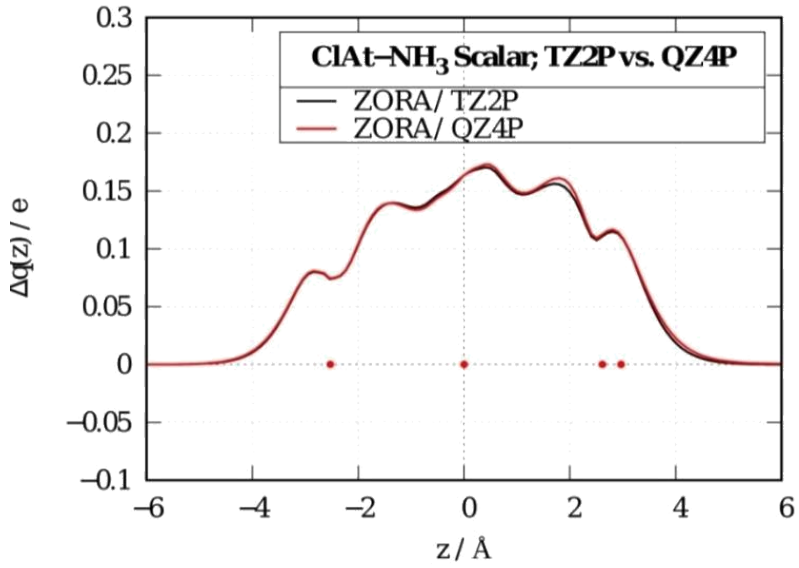

Figure S3: Charge displacement curves for Cl—At ⋯NH_3 at scalar ZORA level with TZ2P (black line) and QZ4P (red line) basis sets. All the calculations have been done with the GGA BP86 functional and core none. Black/red points represent, from the left to the right, the positions of the Cl, At, N and H atoms in the ZORA/TZ2P and ZORA/QZ4P geometries, respectively.

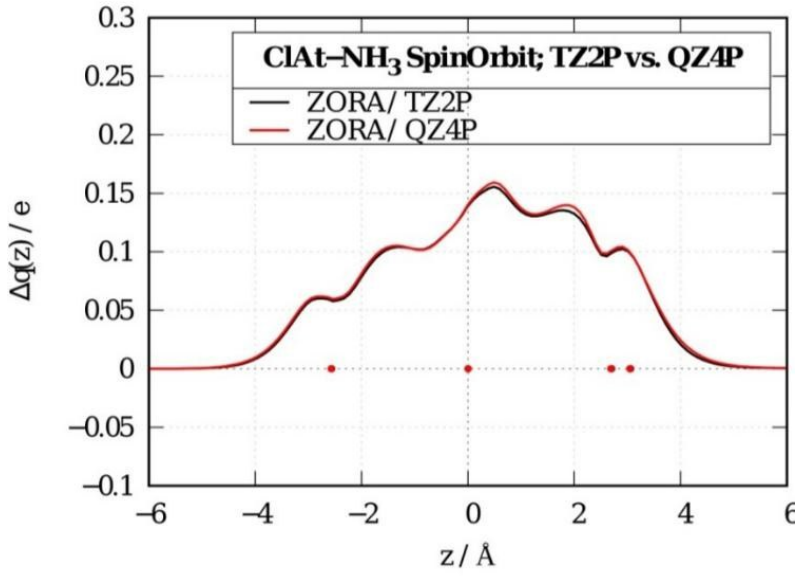

Figure S4: Charge displacement curves for Cl—At ···NH_3 at ZORA SOC level with TZ2P (black line) and QZ4P (red line) basis sets. All the calculations have been done with the GGA BP86 functional and core none. Black/red points represent, from the left to the right, the positions of the Cl, At, N and H atoms in the ZORA/TZ2P and ZORA/QZ4P geometries, respectively.

The two CD curves overlap in both Figure S3 and Figure S4, indicating that the basis set size does not affect the CD analysis. However, a slightly different shape of the CD curve is observed at the ZORA SOC level, particularly at the Cl—At side, suggesting sizable effect of SOC on At. The corresponding Charge Transfer CT values calculated at the isodensity boundary are reported in Table S7 and they are also very close for the two different basis sets. However, it is interesting to note that inclusion of SOC decreases the CT values by 0.019 e. Thus, the SOC effect is larger than the basis set size one.

	TZ2P	QZ4P
	CT	CT
Scalar	**0.151**	**0.153**
SOC	**(0.132)**	**(0.134)**
ΔSO	**-0.019**	**-0.019**

Table S7: Charge transfer values (CT) (electrons) obtained from the CD analysis at both scalar ZORA and ZORA SOC level for the Cl—At $\cdots NH_3$ adduct with TZ2P and QZ4P basis sets. All the calculations have been done with the GGA BP86 functional and the core none.

In conclusion, based on the non-convergence of the bonding energy values calculated with the two different basis sets, the largest size ZORA/QZ4P is selected for our systematic study to guarantee the higher accuracy of the results.

3 The integration accuracy

Many integrals in the ADF program are calculated via numerical integration. The integration grid used for computing these integrals is therefore an important technical aspect of an ADF calculation, affecting both the accuracy of the results and the computation time. The default numerical integration grid in ADF is a refined version of the fuzzy cells integration scheme developed by Becke.[4]

We have tested the "Good" and "Verygood" quality of the Becke integration grid and

results are shown in this section. All results presented in the previous sections were obtained with the Good integration quality.

3.1 Bonding energies

The accuracy of the integration quality (Good and Verygood) is tested in combination with the use of all electron ZORA/QZ4P basis set. Results for bonding energy values are reported in Table S8 in the Cl—At $\cdots NH_3$ adduct.

Numerical quality :	**Good**	**Verygood**	**Literature values**
	BE	**BE**	
Scalar	**-16.95**	**-16.99**	**-15.36** [1]
SOC	**(-13.96)**	**(-14.00)**	**(-13.30)** [2]
ΔSO	**2.99**	**2.99**	**2.37** [2]

Table S8: Bonding energies (scalar ZORA and ZORA SOC) (kcal/mol) between Cl—At and NH_3 in the Cl—At $\cdots NH_3$ adduct. Calculations have been done with the GGA BP86 functional and the all electron ZORA/QZ4P basis set. Literature values are: counterpoise corrected CCSD(T)-F12b/VTZ-F12 stabilization energy[1] and sr-PW6B95/AVTZ stabilization energy[2].

The values of bonding energy in Table S8 differ by only 0,04 kcal/mol, going from the numerical quality Good to Verygood. The same value of the ΔSO is also calculated.

3.2 Geometry

The integration quality effect on the equilibrium geometry is presented in Table S9 for the Cl—At ···NH_3 adduct. The optimized bond distances calculated at both scalar ZORA and ZORA SOC level using the all electron QZ4P basis set are shown.

Numerical quality :	**Good**		**Verygood**		**Literature**	**values**
	Cl-At	**At···N**	**Cl-At**	**At···N**	**Cl—At**	**At···N**
Scalar	**2.524**	**2.615**	**2.525**	**2.610**	**2.479** [1]	**2.630** [1]
SOC	**(2.571)**	**(2.689)**	**(2.570)**	**(2.692)**	**(2.536)** [2]	**(2.693)** [2]
ΔSO	**0.047**	**0.074**	**0.045**	**0.082**	**0.045** [2]	**0.078** [2]

Table S9: Distances (Å) in the Cl—At···NH_3 adduct. All the calculations have been done with the GGA BP86 functional and the all electron ZORA/QZ4P basis set. Literature values are: counterpoise corrected CCSD(T)-F12b /VTZ-F12 optimized intermolecular and intrahalogen bond lengths (Å) [1] and sc-PW6B95/AVTZ optimized intermolecular and intrahalogen bond lengths(Å) [2].

Only small variations for the distance values can be observed. A +0,008 Å difference is

found for the At···N distance between the Verygood and Good integration quality, while an even smaller +0,002 Å difference is calculated for the Cl—At distance.

The bonding energy and geometry results show that convergence between the two types of numerical quality has been reached. Since computation times increases using the Verygood quality integration, with no significant accuracy improvement over the Good quality results, we chose to employ the integration quality Good. Furthermore these results support the evidence that the non-convergence for bonding energy values is indeed due to the different basis set size.

4 Effect of the exchange-correlation functional

In the DFT approach different density functional approximations can be used for the exchange-correlation term in the Kohn-Sham equations. Recent theoretical benchmark investigations on astatine species have been performed by considering an extensive set of widely used functionals.[5] The hybrid meta-generalized gradient approximation (meta-GGA) PW6B95 functional has been suggested as the best choice as well as the range-separated HSE06 one to study astatine species. The popular and widely used PBE0 and B3LYP hybrid GGA functionals have been found as competitive choices, whereas all functionals having a high fraction of "exact" exchange (for instance M06-2X, M11) have been observed to deliver large errors. Among the GGA functionals, the BP86 has been revealed reasonably reliable in calculating geometries and thermodynamic properties.

In this section a comparison between results obtained with two functionals: the GGA BP86,[6] used for all the previous sections calculations, and the hybrid B3LYP,[7] is made to test if the SOC effects could be dependent on the functional choice. The BP86 is a GGA functional which includes, in addition to the LDA part, terms depending on derivatives (gradients) of the charge density. The B3LYP is a hybrid functional and it contains some combination of a standard GGA with a part of Hartree-Fock exchange. Selection of these two functionals, which are representative of the GGA and hybrid-types, has been based on their widespread use and, for B3LYP, on its accuracy for describing astatine species properties.[5] Our preference for the GGA BP86 over the best

performing meta-hybrid PW6B95, instead, has been dictated by the fact that GGA BP86, at a variance with PW6B95, is implemented in all the currently available DFT-based codes. The whole Cl—X···NH_3 (X = Cl, Br, I and At) adduct series has been considered for this functional benchmark investigation.

4.1 Geometry

The functional effect on the equilibrium geometry has been investigated in the Cl—X ···NH_3 (X = Cl, Br, I and At) adduct series. In Table S10 the optimized bond distances calculated at both the scalar ZORA and ZORA SOC level in conjunction with the all electron ZORA/QZ4P basis set and integration quality Good with the two different functionals (GGA BP86 and hybrid B3LYP) are shown.

	GGA	**BP86**	**Hybrid**	**B3LYP**	**Literature**	**values**
	Cl—X	**X···N**	**Cl—X**	**X···N**	**Cl—X**	**X···N**
Cl-Cl···NH_3						
Scalar	**2.115**	**2.384**	**2.075**	**2.522**	**2.017** [1]	**2.676** [1]
SOC	**(2.115)**	**(2.384)**	**2.075**	**2.521**	**/**	**/**
ΔSO	**< 0.001**	**< 0.001**	**< 0.001**	**-0.001**	**/**	**/**
Cl-Br···NH_3						
Scalar	**2.266**	**2.423**	**2.244**	**2.490**	**2.194** [1]	**2.529** [1]
SOC	**(2.268)**	**(2.425)**	**(2.246)**	**(2.492)**	**/**	**/**
ΔSO	**0.002**	**0.002**	**0.002**	**0.002**	**/**	**/**
Cl-I···NH_3						

Scalar	**2.436**	**2.567**	**2.424**	**2.606**	**2.383** [1]	**2.605** [1]
SOC	**(2.443)**	**(2.580)**	**(2.432)**	**(2.623)**	/	/
ΔSO	**0.007**	**0.013**	**0.008**	**0.017**	/	/
Cl-At···NH_3						
Scalar	**2.524**	**2.615**	**2.519**	**2.639**	**2.479** [1]	**2.630** [1]
SOC	**(2.572)**	**(2.689)**	**(2.568)**	**(2.736)**	**(2.536)** [2]	**(2.693)** [2]
ΔSO	**0.047**	**0.074**	**0.049**	**0.097**	**0.045** [2]	**0.078** [2]

Table S10: Distances (Å) in the Cl—X···NH_3 (X = Cl, Br, I and At) adduct series. All the calculations have been done at both scalar ZORA and ZORA SOC level using the all electron ZORA/QZ4P basis set and the integration quality Good with GGA BP86 and hybrid B3LYP functionals. Literature values are: counterpoise corrected CCSD(T)-F12b /VTZ-F12 optimized intermolecular and intrahalogen bond lengths (Å) [1] and sc-PW6B95/AVTZ optimized intermolecular and intrahalogen bond lengths(Å) [2] .

From Table S10 it can be seen that, as a general trend, the GGA BP86 gives larger Cl—X bond distances and shorter X···N distances than the hybrid B3LYP. The SOC effects are relevant only for the Cl—At···NH_3 adduct. The BP86 and B3LYP ΔSO values for the Cl—At bond are however very close, whereas those for the At···N distances are much different.

4.2 Bonding Energies

The GGA BP6 and hybrid B3LYP functionals are tested in combination with all electron ZORA/QZ4P basis set and integration quality Good at both scalar ZORA and ZORA SOC level. Results for bonding energy values are reported in Table S11 in the whole Cl—X ···NH_3 (X = Cl, Br, I and At) adduct series in order to explore the overall

trend.

	GGA BP86 BE	Hybrid B3LYP BE	Literature values
Cl—Cl···NH_3			
Scalar	**-8.66**	**-5.80**	**- 4.77** [1]
SOC	**(-8.66)**	**(-5.80)**	**/**
ΔSO	**0.00**	**0.00**	**/**
Cl—Br···NH_3			
Scalar	**-12.73**	**-9.84**	**-9.06** [1]
SOC	**(-12.67)**	**(-9.82)**	**/**
ΔSO	**0.06**	**0.02**	**/**
Cl—I ···NH_3			
Scalar	**-14.34**	**-12.00**	**-12.24** [1]
SOC	**(-13.88)**	**(-11.64)**	**/**
ΔSO	**0.46**	**0.36**	**/**
Cl—At···NH_3			
Scalar	**-16.95**	**-14.96**	**-15.36** [1]
SOC	**(-13.96)**	**(-12.45)**	**(-13.30)** [2]
ΔSO	**2.99**	**2.51**	**2.37** [2]

Table S11: Bonding energies (scalar ZORA and ZORA SOC) (kcal/mol) between Cl-X and NH_3 in the Cl—X···NH_3 (X = Cl, Br, I and At) adduct series. Calculations have been performed with the GGA BP86 and hybrid B3LYP functionals in combination with the all electron ZORA/QZ4P basis set and the integration quality Good at the corresponding BP86 and B3LYP optimized geometries. Literature values are: counterpoise corrected CCSD(T)-F12b/VTZ-F12 stabilization energy[1] and sr-PW6B95/AVTZ stabilization energy[2].

The following trends can be observed: i) both at the scalar ZORA and ZORA SOC level GGA BP86 bonding energy values are larger than the B3LYP ones; ii) the SOC effects are negligible for Cl—Cl···NH_3 and Cl—Br···NH_3 and increasingly important from Cl—I···NH_3 to Cl—At···NH_3 (see ΔSO values in Table S11). Notably, the increasing bonding energy values trend along the adduct series reported in the literature[5] is reproduced by both the functionals.

It is interesting to note that, in the lighter halogen adducts (i.e. Cl and Br), the BP86 bonding energy values are sizably larger than the literature values, at a variance with B3LYP ones. For the heavier halogen adducts (i.e. I and At), the difference between the BP86 and literature bonding energy values tends to decrease: in Cl—At ···NH_3 , for instance, the BP86 bonding energy differs from the literature value by only about 1 kcal/mol.

4.3 Dipole Moment

The SOC effects can be as important as the electron correlation and can largely affect the chemical properties of astatine species. For instance, it has been suggested that SOC reverses the bond polarization (i.e. the dipole moment) in the HAt compound.[8] Hence, it is interesting to investigate the functional dependence and the SOC effects on the dipole moment in the Cl—X (X = Br, I and At) adduct series. Focusing on the values in the dimers, indication about how much the charges separation is influenced by the different functionals can be obtained.

The GGA BP6 and hybrid B3LYP functionals are used in conjunction with all electron ZORA/QZ4P basis set and integration quality Good at both scalar ZORA and ZORA SOC level. Calculated dipole moment values are reported in Table S12.

	GGA BP86	**hybrid B3LYP**
	M	**M**
Cl—Br		
Scalar	**0.507**	**0.540**
SOC	**(0.533)**	**(0.564)**
ΔSO	**0.026**	**0.024**
Cl—I		
Scalar	**1.077**	**1.171**
SOC	**(1.227)**	**(1.328)**
ΔSO	**0.150**	**0.157**
Cl—At		
Scalar	**1.695**	**1.840**
SOC	**(2.598)**	**(2.817)**
ΔSO	**0.903**	**0.977**

Table S12: Dipole moments (scalar ZORA and ZORA SOC) (Debye) of the Cl—X (X = Cl, Br, I and At) dimer series. Calculations have been performed with the GGA BP86 and hybrid B3LYP functionals using the all electron ZORA/QZ4P basis set and the integration quality Good.

Notably, although larger dipole moments are computed with hybrid B3LYP than those obtained with GGA BP86, the same trend can be found at both scalar ZORA and ZORA SOC level using the two functionals, with SOC values strongly increasing from Cl—I to Cl—At .

4.4 Charge Displacement analysis

The functional effect on the CD analysis is illustrated in Figure S5, where CD curves obtained using GGA BP86, hybrid B3LYP and hybrid B3LYP functional at the BP86 optimized geometry for each adduct in the series are compared. The CD curves have been calculated employing the all electron ZORA/QZ4P basis sets with integration accuracy Good at scalar ZORA level (Figure S5, left) and ZORA SOC (Figure S5, right) for the Cl—X $\cdots NH_3$ (X = Cl, Br, I and At) adduct series. For each adduct, at each relativistic level (scalar and SOC), comparison of the three CD curves allows to disentangle the effect of the functional (GGA BP86 vs. B3LYP at the BP86 geometry CD curves) and the effect of the different geometry (B3LYP vs. B3LYP at the BP86 geometry CD curves).

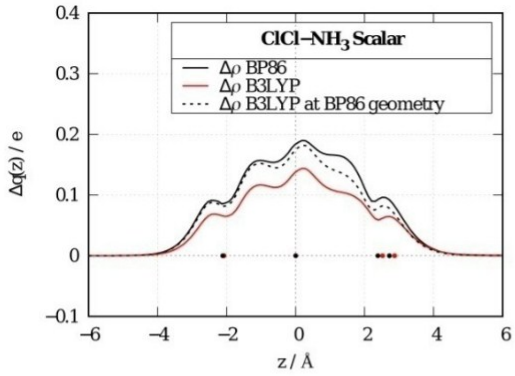
ClCl–NH3 Scalar
Δρ BP86
Δρ B3LYP
Δρ B3LYP at BP86 geometry
Δq(z) / e
z / Å

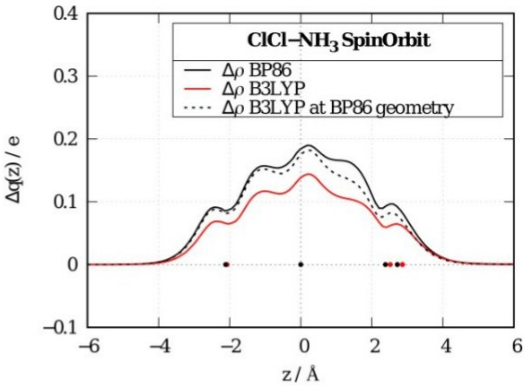
ClCl–NH3 SpinOrbit
Δρ BP86
Δρ B3LYP
Δρ B3LYP at BP86 geometry
Δq(z) / e
z / Å

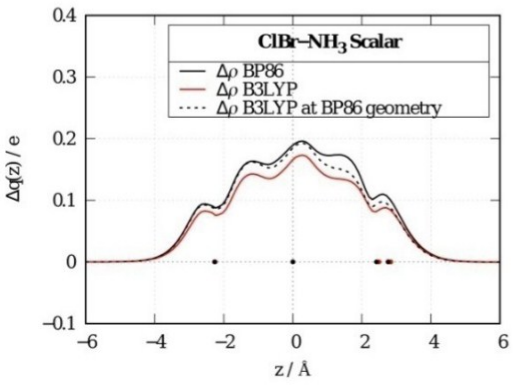
ClBr–NH3 Scalar
Δρ BP86
Δρ B3LYP
Δρ B3LYP at BP86 geometry
Δq(z) / e
z / Å

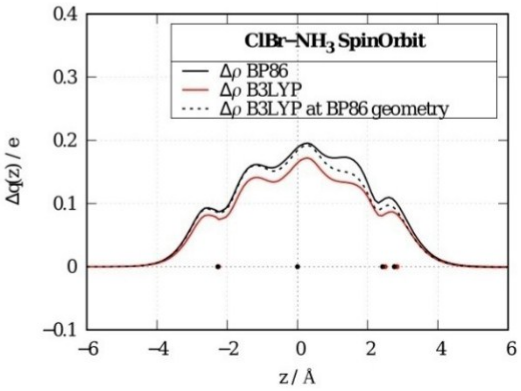
ClBr–NH3 SpinOrbit
Δρ BP86
Δρ B3LYP
Δρ B3LYP at BP86 geometry
Δq(z) / e
z / Å

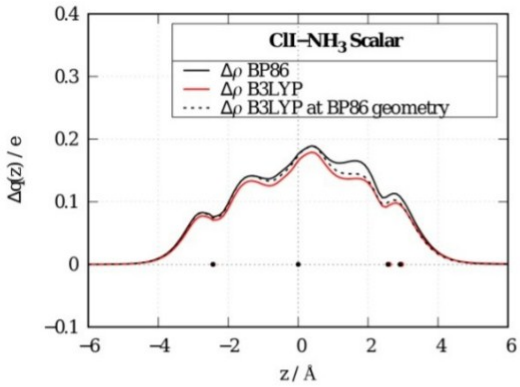
ClI–NH3 Scalar
Δρ BP86
Δρ B3LYP
Δρ B3LYP at BP86 geometry
Δq(z) / e
z / Å

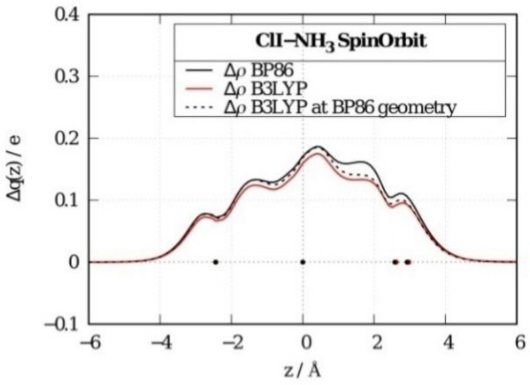
ClI–NH3 SpinOrbit
Δρ BP86
Δρ B3LYP
Δρ B3LYP at BP86 geometry
Δq(z) / e
z / Å

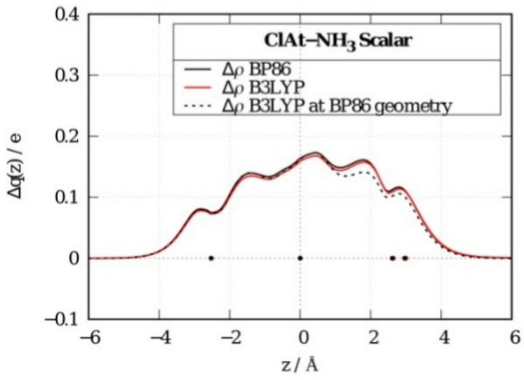
ClAt–NH3 Scalar
Δρ BP86
Δρ B3LYP
Δρ B3LYP at BP86 geometry
Δq(z) / e
z / Å

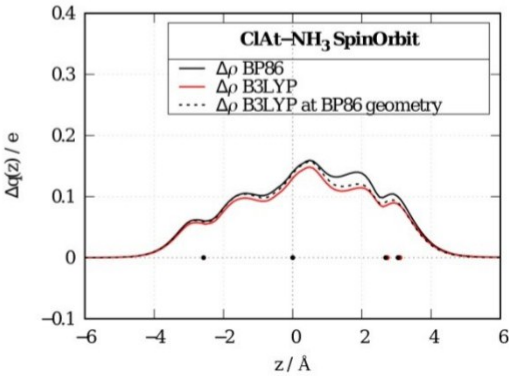
ClAt–NH3 SpinOrbit
Δρ BP86
Δρ B3LYP
Δρ B3LYP at BP86 geometry
Δq(z) / e
z / Å

Figure S5: Charge displacement curves for Cl—X ···NH_3 (X = Cl, Br, I and At, from top to bottom) at scalar ZORA (left column) and ZORA SOC (right column) level with GGA BP86 (black line), hybrid B3LYP (red line) and B3LYP at the BP86 optimized geometry (dotted black line) functionals. All the calculations have been done with the all electron ZORA/QZ4P basis set and integration accuracy Good. Black/red points represent, from the left to the right, the positions of the Cl, At, N and H atoms in the BP86 and B3LYP geometries, respectively.

This series of graphics is particularly useful to immediately visualize trends along the different halogenated adducts. The following trends can be readily observed: i) the CD curves do not show strong dependence on the functional type (compare black curves with dotted black curves in Figure S5); ii) moving down the series towards heavier halogens the geometry effect decreases sizably (compare red curves with dotted black curves in Figure S5), until becoming negligible for the Cl—At···NH_3 adduct; iii) the scalar ZORA and ZORA SOC CD curves have a very similar shape, except for the Cl—At···NH_3 adduct, hence signaling strong SOC effects for it. Notably, variation of the geometry effect on CD curves along the adduct series suggests that no functional can be found which would be simultaneously accurate for describing different systems.

The results of this analysis of the functional effect show an interesting correlation between the CD curves and the bonding energies: when the bonding energies calculated with the two different functionals are similar, the corresponding CD curves tend to coincide.

The corresponding Charge Transfer CT values calculated at the isodensity boundary are reported in Table S13.

	GGA BP86	hybrid B3LYP	B3LYP at the BP86 geometry
	CT(e)	CT(e)	CT(e)
Cl-Cl···NH_3			
Scalar	**0.165**	**0.105**	**0.139**
SOC	**(0.165)**	**(0.105)**	**(0.139)**
ΔSO	**3.00E-04**	**1.00E-04**	**6.34E-05**
Cl-Br···NH_3			
Scalar	**0.174**	**0.135**	**0.152**
SOC	**(0.173)**	**(0.109)**	**(0.152)**
ΔSO	**-5.00E-04**	**-0.026**	**-5.00E-04**
Cl-I···NH_3			
Scalar	**0.163**	**0.137**	**0.145**
SOC	**(0.160)**	**(0.133)**	**(0.142)**
ΔSO	**-0.003**	**-0.004**	**-0.003**
Cl-At···NH_3			
Scalar	**0.153**	**0.149**	**0.135**
SOC	**(0.134)**	**(0.109)**	**(0.117)**
ΔSO	**-0.019**	**-0.040**	**-0.019**

Table S13: Charge transfer values (CT) (electrons) obtained from the CD analysis at the scalar ZORA and ZORA SOC level for the Cl—X···NH_3 (X = Cl, Br, I and At) adducts series with BP86, B3LYP and B3LYP at the BP86 optimized geometry functionals. All the calculations have been done with the all electron ZORA/QZ4P basis set and integration quality Good.

On comparing values in the first and last column of Table S13 we can observe the functional effect. Both at the scalar ZORA and ZORA SOC level a sizable decrease of the CT values calculated with B3LYP with respect to BP86 ones is found. The geometry effect can be seen on comparing values in the second and last column of Table S13. For the Cl—X···NH_3 with X = Cl, Br and I adducts an increase of the CT values is found on going from the B3LYP optimized geometry to the BP86 one, whereas for the Cl—At···NH_3 adduct the trend is reversed at scalar ZORA level. The SOC effect on the CT values can be observed for the Cl—At···NH_3 adduct, showing a sizable decreases with respect to the scalar ZORA ones. Notably, the SOC effect is apparently much larger with the B3LYP functional (at the B3LYP optimized geometry, see CT values in the second column in Table S13) which also gives a remarkable SOC effect for the Cl—Br···NH_3 adduct (ΔSO = -0.026 e), at variance with the BP86 functional and B3LYP at the BP86 optimized geometry results. This finding, however, should not be ascribed to the SOC effect since the CD curves (both the scalar ZORA and the SOC ZORA) have basically the same shape. Rather, it should be ascribed to the different B3LYP and BP86 optimized geometries, particularly at the ammonia side.

In conclusion, from this analysis the same trend in bonding energies, geometries, dipole moments and CT values has been found with both GGA BP86 and hybrid B3LYP functionals.

On the basis of these findings, we chose to perform our systematic study with the GGA BP86 functional. The reason for that is to obtain results to be coherently compared with those from four-component Dirac-Kohn-Sham calculations which have been performed for the NOCV/CD analysis (see text). Indeed, the four-component Dirac-Kohn-Sham calculations have been carried out with the BERTHA code which currently only implements the GGA BP86 functional.

Four-component Dirac-Kohn-Sham calculations - Computational details

The CD analysis has also been applied to quantify the rearrangement of the electron density in the Cl—At ••• NH_3 adduct starting from the two Cl—At and NH_3 fragments, at relativistic four-component Dirac-Kohn-Sham level,[9] using BERTHA code,[10,11,12,13,14] with the following computational set-up. The large component of the basis set for At was generated by uncontracting double-ζ quality Dyall's basis sets[15,16] augmented with the related polarization and correlating functions. Final basis set schemes are as follows: At (25s21p15d9f1g). Large component basis functions for Cl, N and H were derived by decontracting the related def2-svpd[17,18] basis sets available at the "Basis Set Exchange" site.[19] The corresponding small component basis was generated using the restricted kinetic balance relation.[20] For astatine, a previously optimized auxiliary basis set for density fitting was used. For all other elements namely Cl, N and H, accurate auxiliary basis sets were generated using a simple procedure starting from available DeMon[21] Coulomb fitting basis set. It is worth recalling that the Hermite Gaussian Type Functions (HGTFs) used as fitting functions are grouped together in sets sharing the same exponents (analogous scheme is adopted in the nonrelativistic DFT code DeMon).[21] The sets are formed so that to an auxiliary function of a given angular momentum all the functions of smaller angular momentum are associated. Consequently, due to the variational nature of the density fitting procedure implemented, a fitting basis set of increased accuracy can be generated by simply up-shifting the angular momentum in the basis set definition.[22] For Cl, N and H we achieved a fitting basis set of higher accuracy (referred to as A2) simply by up-shifting of two units the angular momentum of all the DeMon Coulomb Fitting definitions. For the sake of clarity, we give the dimension of the Cl atom auxiliary basis sets which is (9s,9p,9d,4f,4g). This assures an accuracy on the Coulomb energy of 0.03 mHartree. The BP86 functional was used. An energy convergence criterion of 10^{-7} Hartree on the total energy was adopted.

EDA analysis

The energy decomposition analysis (EDA) can be applied in this study for a quantitative interpretation of the chemical bond between the Cl—X (X = Cl, Br, I and At) and NH_3 (X = fragments in terms of the three major contributions to their interaction energy, i.e. the electrostatic interaction, the Pauli repulsion and the orbital interaction.

This partition allows to quantify the amount of each of these three contributions (at scalar ZORA level) to the interaction energy in each adduct and, consequently, to verify the presence of reasonable trends. Moreover, the obtained scalar values will be helpful to make predictions on their variations due to the SOC effect.

The results of the EDA analysis of the scalar ZORA interaction energies, carried out on the Cl—X ••• NH_3 (X = Cl, Br, I and At) adducts, are reported in Table S14.

	Cl-Cl•••NH_3	Cl-Br•••NH_3	Cl-I•••NH_3	Cl-At•••NH_3
ΔE_{Pauli}	39.98	46.54	46.20	44.35
ΔE_{elstat}	-25.27	-32.86	-35.68	-38.06
ΔE_{oi}	-25.60	-28.36	-26.16	-24.27
ΔE_{int}	-10.89	-14.68	-15.64	-17.98

Table S14: Interaction energies ΔE_{int} and their decomposition terms (ΔE_{Pauli} , ΔE_{elstat} and ΔE_{oi}) (scalar ZORA) (kcal/ mol) between Cl—X and NH_3 in the Cl—X•••NH_3 (X = Cl, Br, I and At) adduct series.

Note that the interaction energies ΔE_{int} between the Cl—X and NH_3 fragments in the geometry they have in the adduct are larger than the corresponding bonding energy ΔE between the two separated fragments (Table 1 in the text). Indeed, the interaction energy takes into account the amount of energy involved in the geometry rearrangement of the fragments, namely the preparation term ΔE_{prep} ($\Delta E = \Delta E_{int} + \Delta E_{prep}$) (see Methodology section). This additional contribution to the scalar ZORA energy of the adducts spans a range from the minimum value of 1.03 kcal/mol (Cl—At••• NH_3) up to a maximum of 2.23 kcal/mol (Cl—Cl••• NH_3).

From Table S14, one can observe that in the Cl—Cl•••NH_3 adduct, with a zero dipole moment between the two identical halogens (Cl—Cl), the electrostatic contribution ΔE_{elstat} is clearly substantially smaller than that in the other adducts. Simultaneously, moving from bromine to astatine, an increase of the electronegativity difference between the halogen atoms in the adducts occurs, and consequently a larger (more negative) electrostatic contribution is observed.

On comparing adducts with a non zero dipole moment between the two bonded halogens, the Pauli repulsion energy contribution ΔE_{Pauli} decreases with the increasing size of the X halogen (X = Br, I and At) bounded to chlorine.

The total orbital interaction energy ΔE_{oi} values decrease from Cl—Br•••NH_3 to Cl—At•••NH_3 as the halogen becomes larger. We should recall here that this energy contribution accounts for electron pair bonding, charge transfer and polarization. The orbital interaction energy trend could be rationalized on the basis of a smaller amount of charge transferred from NH_3 to Cl—X. Note that the value calculated for the Cl—Cl•••NH_3 adduct deviates from the observed trend: its orbital interaction energy value is close to the one of Cl—I•••NH_3. The reason for that could be still based on its different electrostatic.

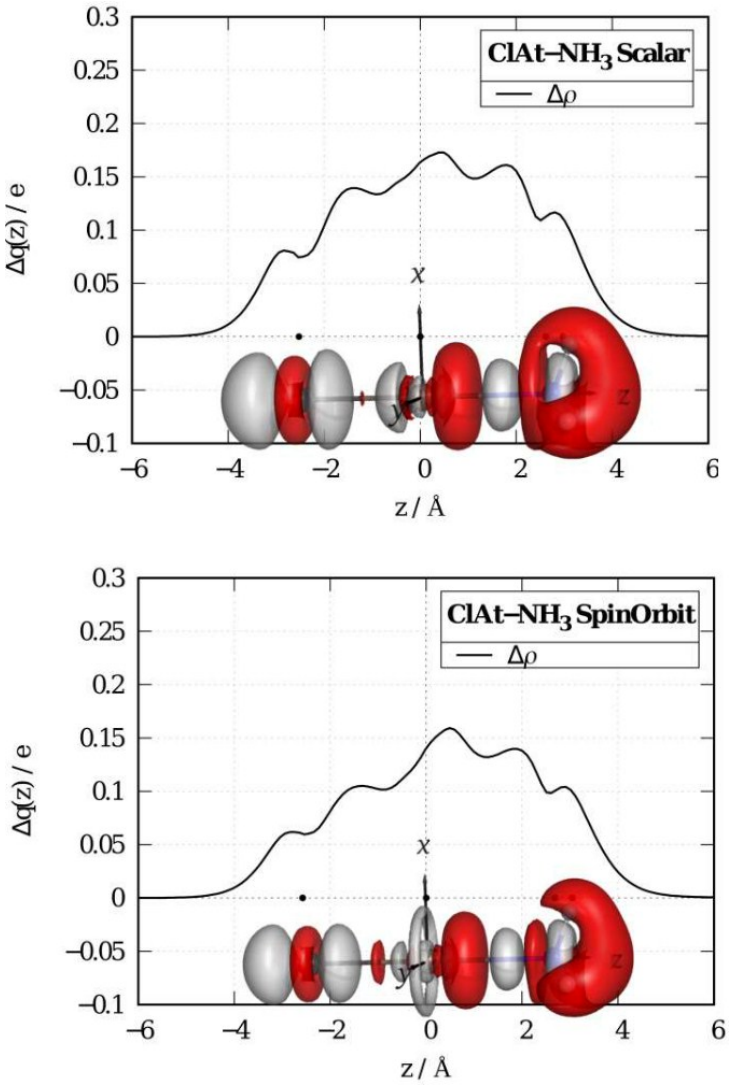

Figure S6: CD curves for the Cl—At•••NH_3 adduct calculated at scalar ZORA (top) and ZORA SOC (bottom) level. Black points represent, from the left to the right, the positions of the Cl, At, N and H atoms, respectively. Isodensity surfaces (± 0.001 e $bohr^{-3}$) of the total density difference Δρ are also shown. Red surfaces represent charge depletion regions and grey surfaces identify charge accumulation regions.

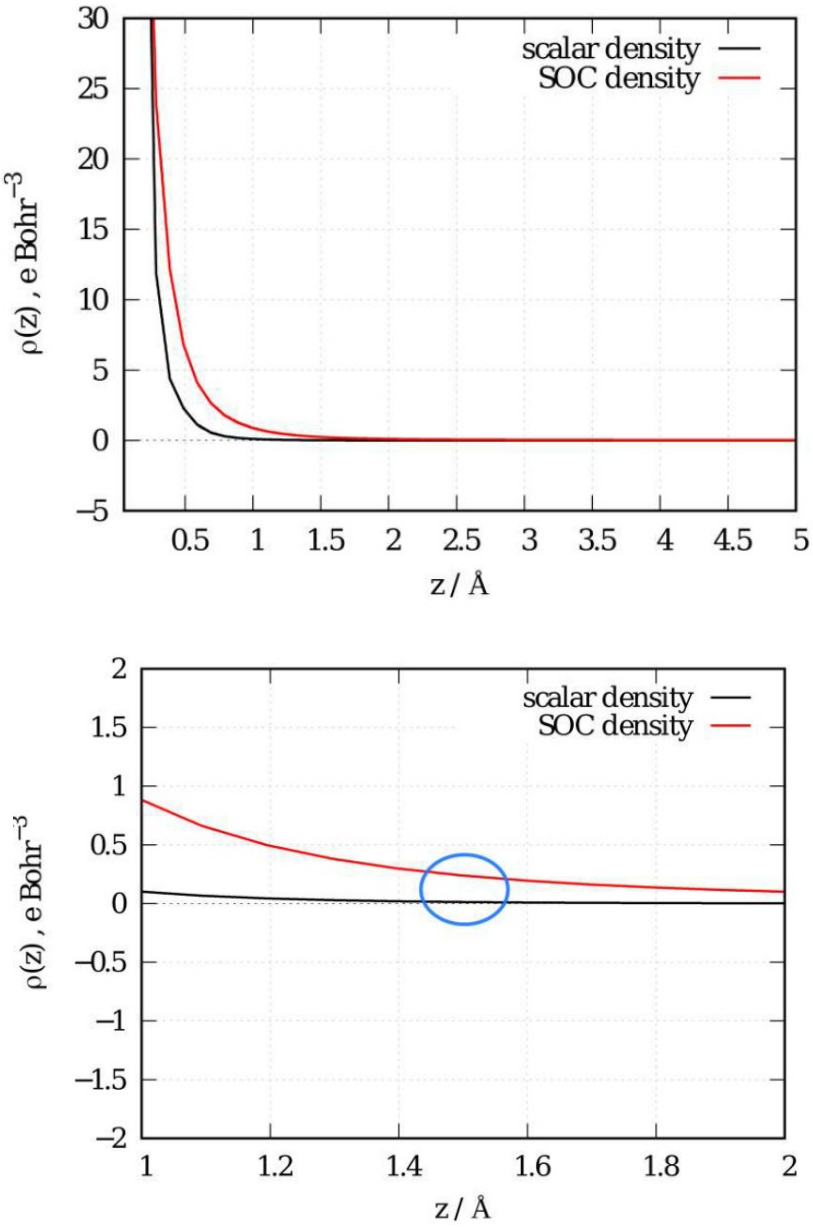

Figure S7: top) electron density (e bohr^{-3}) plotted as a function of the Cl-At/NH_3 distance (Å) at the scalar ZORA level (black line) and SOC ZORA level (red line) for the Cl—At •••NH_3 adduct; bottom) enlargement of the electron density (e bohr^{-3}) trend around the isodensity boundary region (1.441 Å).

As one can see, the SOC electron density is always larger than the scalar one. At any spatial distance the ammonia perceives the electronic density of the Cl—At fragment as enlarged with respect to what can be predicted by the scalar calculations. The enlargement in Figure S7 (bottom) highlights the difference between the scalar ZORA

electron density and the SOC ZORA electron density evaluated at the point where the density of the Cl—At fragment is tangent to the one of the NH_3, the so called isodensity boundary. The SOC ZORA value of the isodensity is calculated to be 1.441 Å. Evaluation of the difference at this point allows to quantify the increase of the electronic density experienced by the ammonia fragment while it gets closer to the Cl—At fragment during the formation of the halogen bond.

The encircled region of the plot in Figure S7 displays the difference between the two electron densities (SOC density – scalar density) evaluated at the isodensity which is about 0.3 e $bohr^{-3}$.

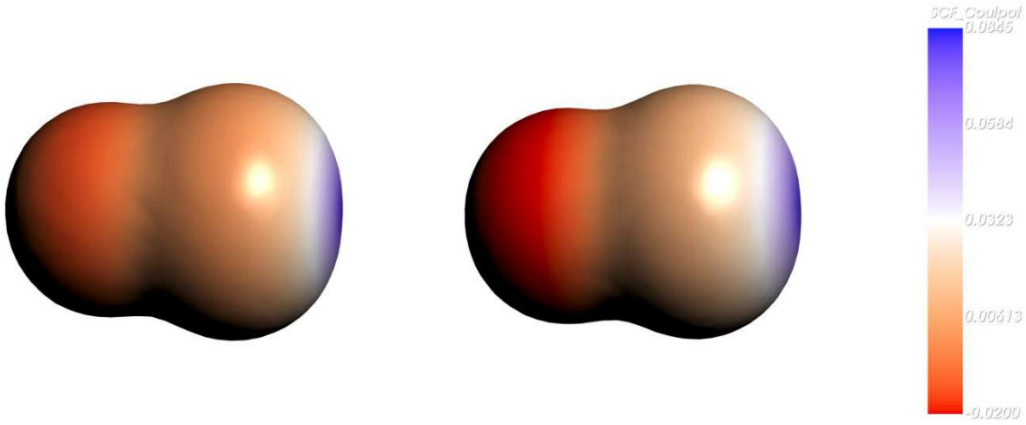

Figure S8: 3D maps of the Coulomb potential at the 0.001 e $bohr^{-3}$ isodensity surface of Cl—At dimer at the scalar ZORA level (left) and SOC ZORA level (right). The values of the potential on this isodensity ranges from - 0.0200 Hartree/e (bottom of the bar on the right) up to 0.0845 Hartree/e (top of the bar on the right).

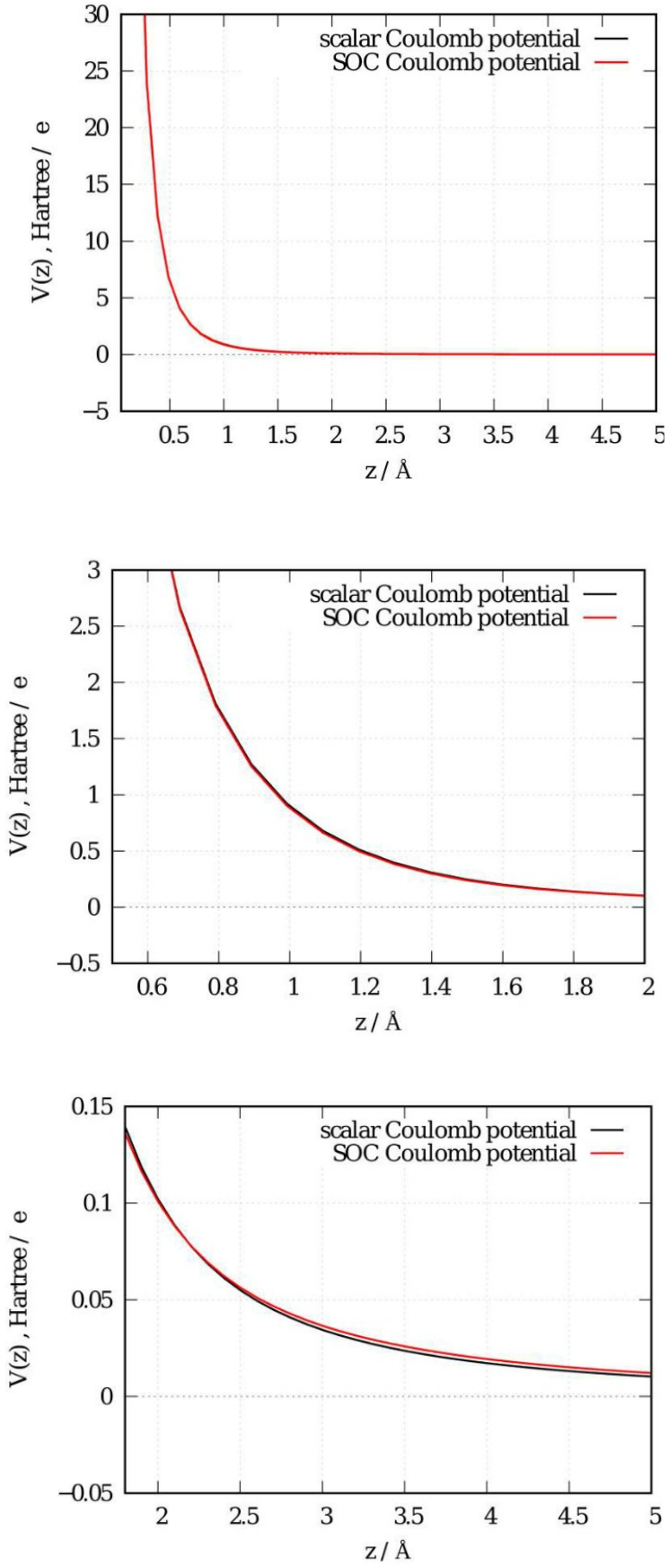

Figure S9: top) Coulomb potential (Hartree/e) plotted as a function of the Cl—At/NH_3 distance (Å) at

the scalar ZORA level (black line) and SOC ZORA level (red line) for the Cl—At•••NH_3 adduct; middle) trend enlargement at short range; bottom) trend enlargement at long range.

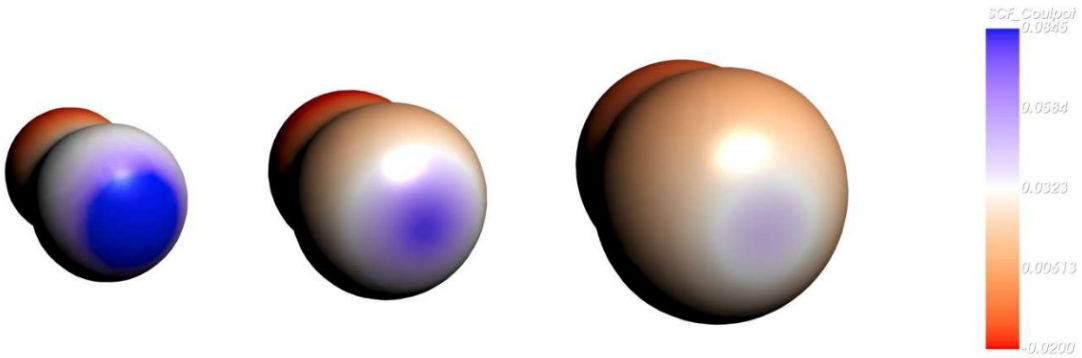

Figure S10: 3D map of the Coulomb potential at the 0.005 e $bohr^{-3}$ (left), 0.001 e $bohr^{-3}$ (middle) and 0.0001 e $bohr^{-3}$ (right) isodensity surfaces of Cl—At at the SOC ZORA level. The values of the potential ranges from - 0.0200 Hartree/e (bottom of the bar on the right) up to 0.0845 Hartree/e (top of the bar on the right). The molecule is orientated to focus on the astatine side.

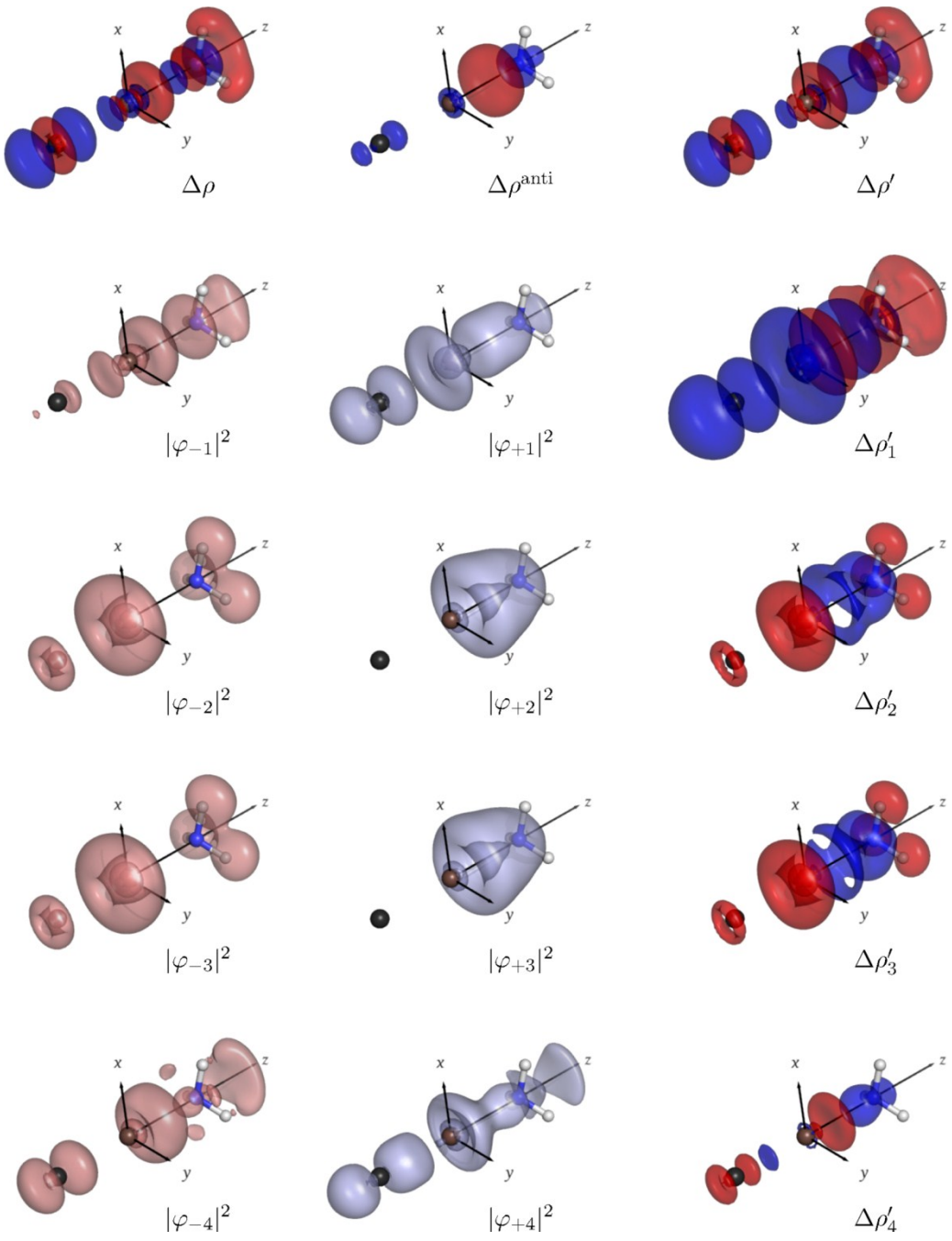
$\Delta\rho$
$\Delta\rho^{\mathrm{anti}}$
$\Delta\rho'$
$|\varphi_{-1}|^2$
$|\varphi_{+1}|^2$
$\Delta\rho'_1$
$|\varphi_{-2}|^2$
$|\varphi_{+2}|^2$
$\Delta\rho'_2$
$|\varphi_{-3}|^2$
$|\varphi_{+3}|^2$
$\Delta\rho'_3$
$|\varphi_{-4}|^2$
$|\varphi_{+4}|^2$
$\Delta\rho'_4$

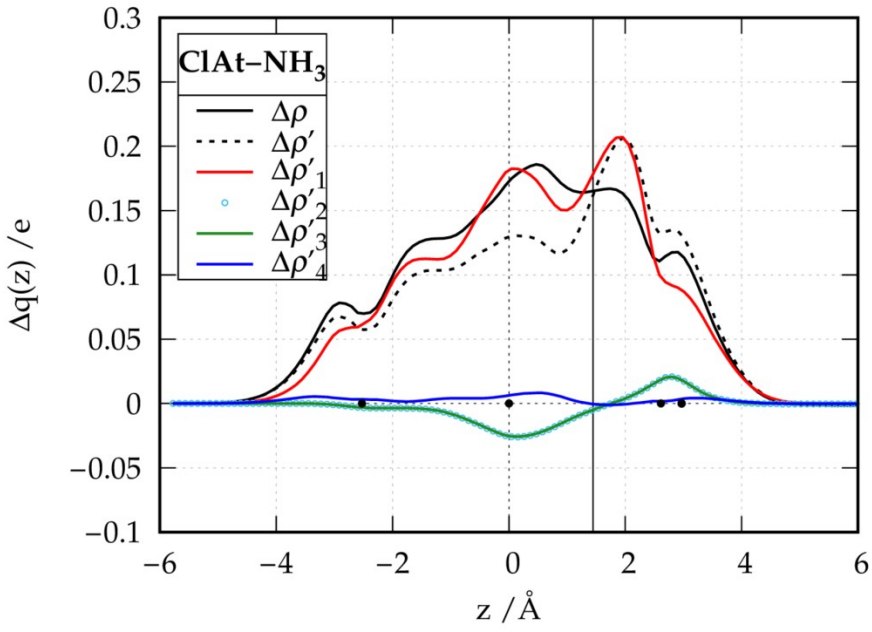
ClAt–NH3
Δρ
Δρ′
Δρ′1
Δρ′2
Δρ′3
Δρ′4
Δq(z) /e
z /Å
0.3
0.25
0.2
0.15
0.1
0.05
0
−0.05
−0.1
−6
−4
−2
0
2
4
6

Figure S11: CD curves for the Cl—At ••• NH_3 bond calculated at relativistic four-component Dirac-Kohn-Sham level with speed of light c = 10 x 137.036 au (non-relativistic limit). Black points represent, from the left to the right, the positions of the Cl, At, N and H atoms. Top: isodensity surfaces (± 0.0014 e $bohr^{-3}$) for $\Delta\rho$, $\Delta\rho'$, and $\Delta\rho_{anti}$. Contribution to $\Delta\rho'$ of the four most significant NOCV-pairs ($\Delta\rho'_1$, $\Delta\rho'_2$, $\Delta\rho'_3$, and $\Delta\rho'_4$) (±0.00015 e $bohr^{-3}$) and NOCV densities ($|\varphi_{+k}|^2$, $|\varphi_{-k}|^2$, k=1,2,3,4) (±0.003 e $bohr^{-3}$). Red surfaces identify charge depletion areas, and blue surfaces identify charge accumulation areas.

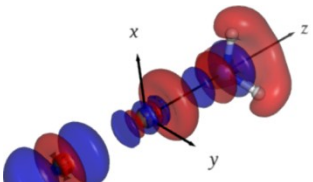

$\Delta\rho$

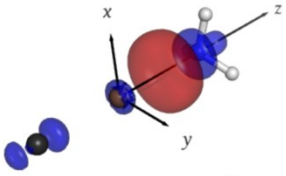

$\Delta\rho^{\mathrm{anti}}$

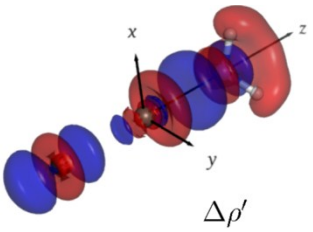

$\Delta\rho'$

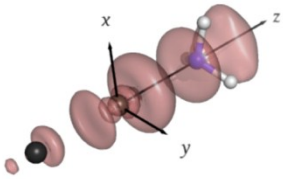

$|\varphi_{-1}|^2$

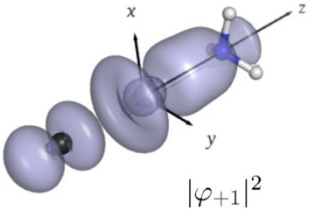

$|\varphi_{+1}|^2$

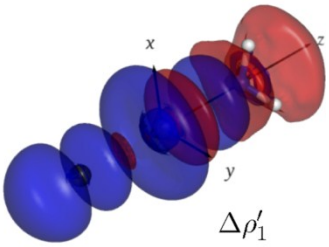

$\Delta\rho'_1$

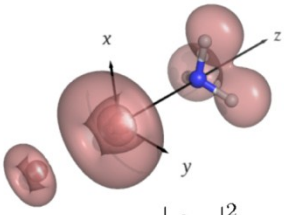

$|\varphi_{-2}|^2$

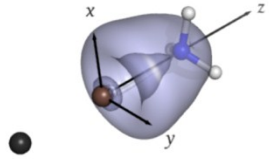

$|\varphi_{+2}|^2$

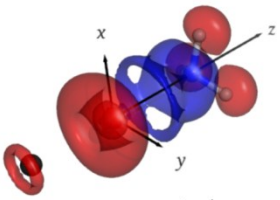

$\Delta\rho'_2$

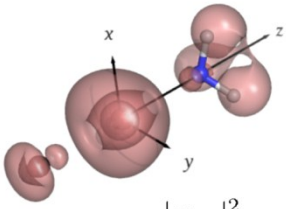

$|\varphi_{-3}|^2$

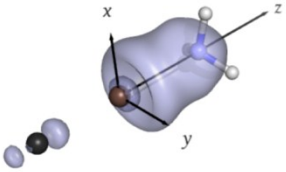

$|\varphi_{+3}|^2$

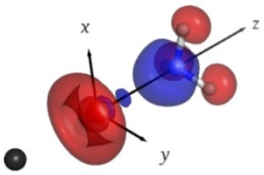

$\Delta\rho'_3$

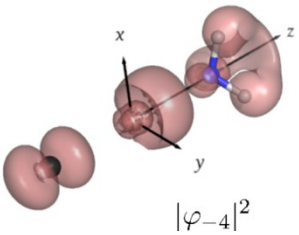

$|\varphi_{-4}|^2$

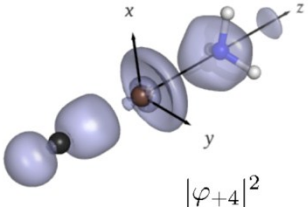

$|\varphi_{+4}|^2$

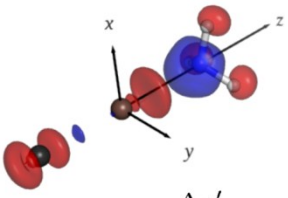

$\Delta\rho'_4$

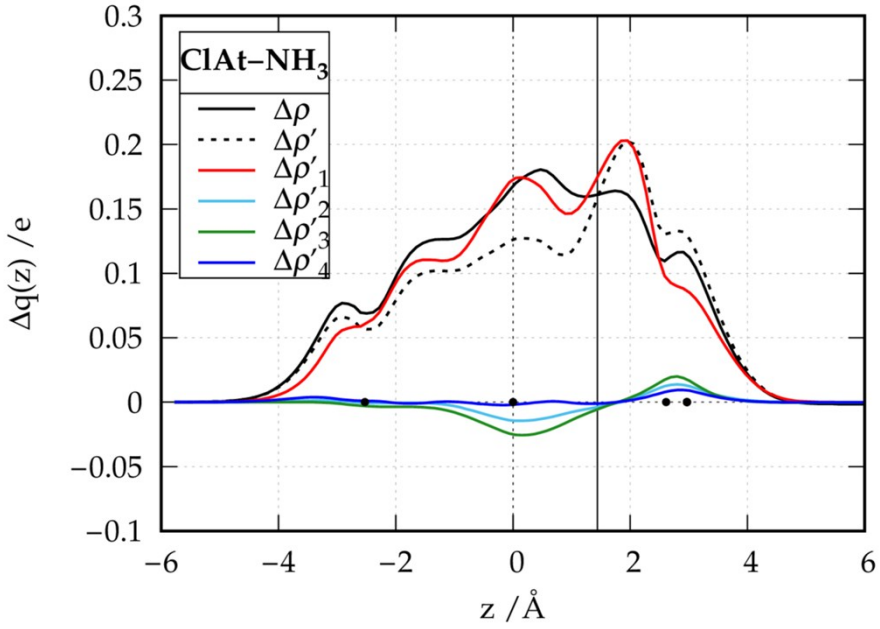

Figure S12: CD curves for the Cl—At ••• NH_3 bond calculated at relativistic four-component Dirac-Kohn-Sham level with speed of light c = 2 x 137.036 au. Black points represent, from the left to the right, the positions of the Cl, At, N and H atoms. Top: isodensity surfaces (± 0.0014 e $bohr^{-3}$) for Δρ, Δρ', and $\Delta\rho_{anti}$. Contribution to Δρ' of the four most significant NOCV-pairs ($\Delta\rho'_1$, $\Delta\rho'_2$, $\Delta\rho'_3$, and $\Delta\rho'_4$) (± 0.00015 e $bohr^{-3}$) and NOCV densities ($|\varphi_{+k}|^2$, $|\varphi_{-k}|^2$, k=1,2,3,4) (± 0.003 e $bohr^{-3}$). Red surfaces identify charge depletion areas, and blue surfaces identify charge accumulation areas.

References

1 J.G. Hill and X. Hu, *Chem. Eur. J.* 2013, **19**, 3620 – 3628.

2 J. Graton, S. Rahali, J.-Y. Le Questel, G. Montavon, J. Pilmé and N. Galland, *Phys. Chem. Chem. Phys.* 2018, **20**, 29616 – 29624.

3 a) C. Fonseca Guerra, J.G. Snijders, G. te Velde and E.J. Baerends *Theor. Chem. Acc*. 1998, **99**, 391-403; b) G. te Velde, F.M. Bickelhaupt, E.J. Baerends, C. Fonseca Guerra, S.J.A. van Gisbergen, J.G. Snijders and T. Ziegler, *J. Comput. Chem.* 2001, **22**, 931-967; c) ADF2016, SCM, Theoretical Chemistry, Vrije Universiteit, Amsterdam, The Netherlands, http://www.scm.com.

4 A.D. Becke, *J. Chem. Phys.* 1988, **88**, 2547.

5 D.-C. Sergentu, G. David, G. Montavon, R. Maurice and N. Galland *J. Comput. Chem.* 2016, **37**, 1345-1354.

6 a) A.D. Becke, *Phys. Rev. A* 1988**, 38,** 3098-3100; b) J. P. Perdew, *Phys. Rev. B* 1986**, 33**, 8822-8824.

7 P.J. Stephens, F.J. Devlin, C.F. Chabalowski and M.J. Frisch, *J. Phys. Chem.* 1994, **98**, 11623-11627.

8 P. Norman, B. Schimmelpfennig, K. Ruud, H. J. A. Jensen and H. Ågren, *J. Chem. Phys*. 2002, **116**, 6914-6923.

9 L. Belpassi, L. Storchi, H.M. Quiney and F. Tarantelli, *Phys. Chem. Chem. Phys.*, 2011, **13**, 12368-12394.

10 H.M. Quiney and P. Belanzoni, *J. Chem. Phys*., 2002, **117**, 5550-5563.

11 H.M. Quiney, H. Skaane and I.P. Grant, *J. Phys. B: At., Mol. Opt. Phys.,* 1997, **30**, L829.

12 H.M. Quiney, H. Skaane and I.P. Grant in *Adv. Quantum Chem*., ed. P.-O. Löwdin, Academic Press, 1998, vol. **32**, pp. 1-49.

13 L. Belpassi, L. Storchi, F. Tarantelli, A. Sgamellotti and H.M. Quiney, *Future Gener. Comput. Syst*., 2004, **20**, 739-747.

14 L. Belpassi, F. Tarantelli, A. Sgamellotti and H.M. Quiney, *J. Chem. Phys*., 2005,

122, 184109.

15 K.G. Dyall, *Theor. Chem. Acc.*, 1998, **99**, 366-371; addendum *Theor. Chem. Acc.* 2002, 108, 365-365; revision *Theor. Chem. Acc.* 2006, **115**, 441-447. Basis sets available from the Dirac website, http://dirac.chem.sdu.dk.

16 K.G. Dyall, *Theor. Chem. Acc.*, 2012, **131**, 1217-1227. Basis sets available from the Dirac website, http://dirac.chem.sdu.dk.

17 D. Rappoport and F. Furche, *J. Chem. Phys*., 2010, **133**, 134105.

18 F. Weigend and R. Ahlrichs, *Phys. Chem. Chem. Phys.*, 2005, **7**, 3297-3305.

19 B.P. Pritchard, D. Altarawy, B.T. Didier, T.D. Gibson and T.L. Windus, *J. Chem. Inf. Model.*, 2019, doi:acs.jcim.9b00725.

20 I.P. Grant and H.M. Quiney, *Phys. Rev. A*, 2000, **62**, 022508.

21 A.M. Köster and D.R. Salahub, *deMon2k*, version 4; Cinvestav, Mexico City, 2016. https://hadoop.apache.org.

22 M. De Santis, L. Belpassi, F. Tarantelli and L. Storchi, *Rendiconti Lincei. Scienze Fisiche e Naturali*., 2018, **29**, 209-217.

Geometries xyz

Cl—At

scalar

2

Cl 0.000000 0.000000 -2.443

At 0.000000 0.000000 0.000

Cl—At

SOC

2

Cl 0.000000 0.000000 -2.516

At 0.000000 0.000000 0.000

Cl—Cl ···NH_3

scalar

6

Cl 0.000000 0.000000 -2.11459

Cl 0.000000 0.000000 0.00000

N 0.000000 0.000000 2.38445

H -0.961607 0.000000 2.71845

H 0.480803 -0.832776 2.71845

H 0.480803 0.832776 2.71845

SOC

6

Cl 0.000000 0.000000 -2.11478

Cl 0.000000 0.000000 0.00000

N 0.000000 0.000000 2.38448

H -0.961610 0.000000 2.71846

H 0.480805 -0.832779 2.71846

H 0.480805 0.832779 2.71846

Cl—Br ···NH_3

scalar

6

Cl 0.000000 0.000000 -2.266

Br 0.000000 0.000000 0.00000

N 0.000000 0.000000 2.42322

H -0.960239 0.000000 2.76173

H 0.480120 -0.831592 2.76173

H 0.480120 0.831592 2.76173

SOC

6

Cl 0.000000 0.000000 -2.26764

Br 0.000000 0.000000 0.00000

N 0.000000 0.000000 2.42531

H -0.960182 0.000000 2.76398

H 0.480091 -0.831542 2.76398

H 0.480091 0.831542 2.76398

Cl—I ···NH_3

scalar

6

Cl 0.000000 0.000000 -2.43601

I 0.000000 0.000000 0.00000

N 0.000000 0.000000 2.56708

H -0.957544 0.000000 2.91664

H 0.478772 -0.829257 2.91664

H 0.478772 0.829257 2.91664

SOC

6

Cl 0.000000 0.000000 -2.44325

I 0.000000 0.000000 0.00000

N 0.000000 0.000000 2.57997

H -0.957283 0.000000 2.9303

H 0.478642 -0.829032 2.9303

H 0.478642 0.829032 2.9303

Cl—At ···NH_3

scalar

6

Cl 0.000000 0.000000 -2.52415

At 0.000000 0.000000 0.00000

N 0.000000 0.000000 2.61466

H -0.477881 0.827715 2.96915

H -0.477881 -0.827715 2.96915

H 0.955763 0.000000 2.96915

SOC

6

Cl 0.000000 0.000000 -2.57151

At 0.000000 0.000000 0.00000

N 0.000000 0.000000 2.68909

H -0.477322 0.826746 3.04722

H -0.477322 -0.826746 3.04722

H 0.954644 0.000000 3.04722